100-GBd Waveguide Bragg Grating Modulator in Thin-Film Lithium Niobate

David Pohl, Andreas Messner, *Member, IEEE*, Fabian Kaufmann, Marc Reig Escalé, Jannis Holzer, Juerg Leuthold, *Fellow, IEEE*, and Rachel Grange

***Abstract*— An integrated electro-optic modulator based on a waveguide Bragg grating in thin-film lithium niobate is introduced. The compact device with a footprint of 10 × 400 μm^2 displays an optical extinction ratio of 53.8 dB at a wavelength of 1555.9 nm in the C-band. With a simple intensity modulation and direct detection scheme, data rates up to 100 Gbit/s are demonstrated with 2-, 4- and 8-level pulse-amplitude modulation formats. The optical filter characteristic of a waveguide Bragg grating modulator suppresses one optical sideband, resulting in inherent single sideband modulation. This enables transmission of a 100 Gbit/s on-off keying signal over 12 km of standard single-mode fiber at 1559.05 nm, without the need for chromatic dispersion compensation.**

***Index Terms*— Thin-film lithium niobate, integrated optics, electro-optic modulator (EOM), optical fiber communication.**

I. Introduction

HIGH-BANDWIDTH electro-optic modulators (EOMs) are key components in optical communication systems [1] and microwave photonics [2], [3]. Future technologies require parallelism through on-chip integration on a small footprint and high data rates at low power consumption, in order to meet the expected demand for 10-Tb/s optical interfaces [4]. Various physical effects have been utilized for integrated EOMs, including the plasma dispersion effect in silicon photonics [5], electro-absorption [6] and the linear electro-optic effect of organic polymers [7] and ferroelectric materials [8].

Out of these ferroelectrics, lithium niobate (LN) is employed for electro-optic modulation since decades and serves as a workhorse in optical telecommunication systems [9]. The recent advent of high quality thin-films of lithium niobate on insulator (LNOI) has leveraged research in photonic integrated circuits on this platform. Enabled by advances in the nanofabrication, integrated Mach-Zehnder (MZ) EOMs with CMOS-compatible driving voltages, symbol rates up to 100 GBd and low insertion and propagation losses have been demonstrated [10], [11]. Devices based on resonant nanophotonic structures such as microring resonators [12], photonic crystals [13] and phase-shifted Bragg gratings [14] were developed in order to decrease the footprint and power consumption compared to MZ-EOMs. However, the finite photon lifetimes of the optical cavities limit the electro-optic bandwidths of resonator based EOMs.

Here, we propose an integrated EOM on LNOI based on a waveguide Bragg grating (WBG) structure for intensity modulation (IM) systems with direct detection (DD). WBGs are the integrated photonics counterparts of the well-known fiber Bragg gratings with applications in wavelength division multiplexing and photonic signal processing [15], [16]. In LNOI, integrated waveguide gratings as well as the linear electro-optic shift of the transmission spectrum have been previously demonstrated [17], [18]. EOMs based on WBGs have small footprints in the order of 10 × 400 μm^2 and offer the possibility for high level parallelization on a single chip while the electro-optic bandwidth is not cavity-photon lifetime limited. Additionally, the on-chip electrodes are typically by more than a factor of 20 smaller than MZ-EOM travelling wave electrodes, which relaxes the microwave engineering requirements and allows for driving in a lumped circuit.

The fabricated WBG modulator on LNOI shows a static optical extinction ratio of 53 dB at 1555.87 nm in the C-band. The measured 3 dB electro-optic bandwidth of the studied device is 60 GHz and we demonstrate data transmission of non-return to zero with on-off keying (NRZ-OOK) signals up to 100 Gbit/s as well as higher-level formats such as 4-level and 8-level pulse-amplitude modulation (PAM). Due to the inherent optical filter characteristics of a WBG, sideband suppression ratios over 10 dB are observed in the optical modulation spectrum. The resulting single sideband (SSB) modulation is known to mitigate the chromatic dispersion induced power fading in an IM/DD system after transmission through uncompensated standard single mode fibers (SMFs) compared to double sideband (DSB) modulation [19], [20]. In here, we demonstrate transmission of a 100 Gbit/s NRZ-OOK signal in a IM/DD system over a SMF of 12 km without any dispersion correction, enabled by the SSB modulation inherent to a WBG modulator.

II. Concept and Device Fabrication

The concept of a WBG modulator is based on the electro-optic shift of the resonant wavelength of an integrated lithium niobate WBG formed between two electrodes [18], see Fig. 1(a). Fig. 1(b) shows the grating section itself, where the periodic change of the effective refractive index along

Manuscript received September 25, 2020; revised November 12, 2020; accepted December 8, 2020. Date of publication December 14, 2020; date of current version December 29, 2020. This work was supported in part by the Swiss National Science Foundation under Grant 179099, in part by the Swiss Space Office, and in part by the European Research Council (ERC) through the European Union's Horizon 2020 Research and Innovation Programme (Chi2-nanooxides) under Grant 714837. *(Corresponding author: David Pohl.)*

David Pohl, Fabian Kaufmann, Marc Reig Escalé, Jannis Holzer, and Rachel Grange are with the Optical Nanomaterial Group, Institute for Quantum Electronics, ETH Zürich, 8093 Zürich, Switzerland (e-mail: dpohl@phys.ethz.ch; grange@phys.ethz.ch).

Andreas Messner and Juerg Leuthold are with the Institute of Electromagnetic Fields, ETH Zürich, 8092 Zürich, Switzerland.

Digital Object Identifier 10.1109/LPT.2020.3044648

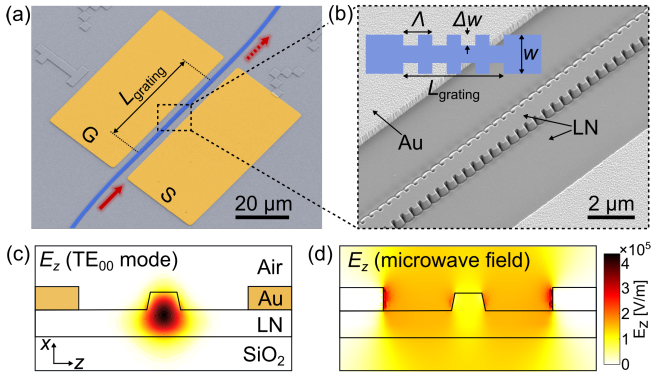

Fig. 1. (a) False-colored SEM image of an integrated WBG modulator. (b) SEM image of the waveguide grating structure. The inset shows a schematic waveguide grating highlighting the geometrical parameters. (c) Simulated electric field component along the crystal z-axis of the fundamental TE-polarized optical mode at a wavelength of 1560 nm. (d) Simulated microwave field component along the z-axis that is induced by applying a voltage of 1 V to the pair of electrodes.

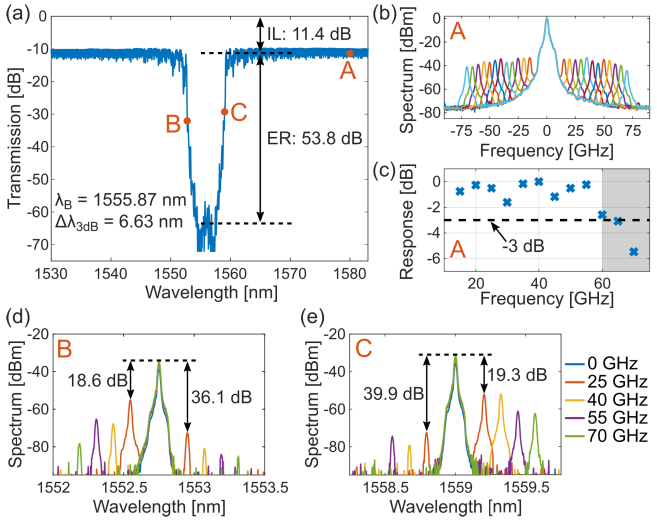

Fig. 2. (a) Optical transmission of the WBG modulator. (b) Optical modulation spectra for a sinusoidal microwave signal at frequencies between 15 GHz and 70 GHz. The optical carrier wavelength is 1580 nm. (c) The 3 dB bandwidth of the RF response of the on-chip electrodes is estimated to be around 60 GHz. (d), (e) Asymmetric optical modulation spectra for different microwave frequencies with the optical carrier at 1552.75 nm (d) (point B in (a)) and at 1559 nm (e) [point C in (a)].

the propagation direction of the optical mode is realized by physical corrugation of the waveguide width [21]. Such WBGs act as wavelength dependent filters with a transmission stopband at the Bragg wavelength $\lambda_B = 2n_{\text{eff}}\Lambda$, where Λ is the grating periodicity and n_{eff} is the effective refractive index of the waveguide mode. In Fig. 1(c) the numerically simulated electric field component along the extraordinary axis of the crystalline LN thin-film (z-axis) of the fundamental TE mode at a wavelength of 1560 nm is plotted in the cross-section of the waveguide. A voltage applied to the pair of electrodes changes the refractive index of the LNOI waveguide. Fig. 1(d) shows the simulated electric field obtained for a voltage of 1 V. By choosing an operational wavelength in the slope of the stopband, an applied electric signal is translated to an intensity modulated optical signal [18].

The WBGs are fabricated on an x-cut LNOI chip with a LN thin-film of 600 nm separated from the silicon substrate by a 2 μm layer of SiO_2. After defining the waveguide structures including the corrugated gratings via electron-beam lithography with HSQ as the resist, the LN thin-film is partially dry-etched by 220 nm with an optimized argon plasma process in an inductively coupled plasma system. Wet-etching in buffered oxide etch and potassium hydroxide removes the remaining mask and residual material from the dry-etching process. Finally, the 300 nm thick gold electrodes with a separation of 6 μm are deposited along the grating section using a lift-off procedure.

A false-colored scanning electron microscope (SEM) image of a fabricated WBG modulator device is shown in Fig. 1(a) and Fig. 1(b) displays a zoomed-in SEM image of the corrugated waveguide grating section. The inset in Fig. 1(b) is a schematic of a waveguide grating with all the relevant geometrical parameters defining the filter characteristics, namely the grating period Λ, the waveguide width w, the corrugation width Δw and the total length of the grating section L_{grating}. The results presented in this work were obtained from a device with the following parameters: $\Lambda = 410$ nm, $w = 1$ μm, $\Delta w = 200$ nm, $L_{\text{grating}} = 410$ μm and with 420 μm long gold electrodes.

III. Device Characterization

As a first device characterization, the optical transmission of the WBG modulator is measured. Light from a tunable laser source (TLS) is end-fire coupled in and out of the chip using lensed fibers. The input polarization is adjusted via a fiber polarization controller to predominantly couple to the fundamental TE mode of the waveguide. This ensures that the optical and microwave electric fields are aligned to the z-axis of the LN layer, in order to maximize the electro-optic response of the device. The transmission spectrum of the WBG modulator is measured with an optical power meter and shown in Fig. 2(a). The measured resonant Bragg wavelength is $\lambda_B = 1555.87$ nm and the 3 dB bandwidth of the stopband is $\Delta\lambda_{3\text{dB}} = 6.63$ nm. The suppression of the signal at the Bragg wavelength is 53.8 dB and the fiber-to-fiber insertion loss in the transmitting spectral parts is 11.4 dB, which is mainly due to fiber-to-chip coupling losses, while the on-chip losses account only for 0.2 dB.

The linear electro-optic tuning efficiency of the Bragg wavelength is measured using a phase-shifted WBG with identical design parameters as the studied modulator device and fabricated on the same chip. The narrow cavity resonance of the phase-shifted WBG (Q-factor of $\sim 2 \times 10^5$) allows to monitor the electro-optic shift more accurately than the wide stopband of a single WBG does. By recording the transmission spectra for different applied DC voltages, a linear tuning efficiency of 14.6 pm/V is obtained [22].

Subsequently, the RF frequency response of the on-chip electrodes is studied. Therefore, the device is driven at an operating wavelength of 1580 nm, where the filter response of the Bragg grating can be assumed to be negligible [point A in Fig. 2(a)]. Then, the electrodes are contacted with a ground-signal (GS) RF probe and a sinusoidal microwave signal is applied, which induces an optical phase shift. The phase

moduation gives rise to symmetric optical sidebands measured with an optical spectrum analyzer (OSA) [23]. In Fig. 2(b) the recorded optical spectra for microwave frequencies from 15 to 70 GHz are plotted. From the relative power levels of the first sidebands at each microwave frequency and by taking the cable and RF probe losses into account, the 3 dB bandwidth of the electrode pair was found to be above 60 GHz, see Fig. 2(c). The RF frequency response could be improved by optimizing the electrode design, especially by decreasing the number of grating periods and hence the length of the electrodes.

Next, the sideband suppression is studied by tuning the laser wavelength to one of the slopes of the stopband [points B and C in Fig. 2(a)]. Now, the generated modulation sidebands are partially suppressed by the filter response of the WBG modulator. This results in asymmetric optical spectra where either the left or the right sidebands are suppressed, depending on the operational wavelength, see Fig. 2(d) and Fig. 2(e). For a laser wavelength of 1559 nm and a microwave frequency of 25 GHz, the first order sideband on the left side of the carrier is suppressed by 20.6 dB compared to the right one. Measurements at increasing carrier wavelengths showed that the WBG modulator suppresses the left sidebands by at least 6 dB up to 1559.25 nm at the right edge of the stopband. Vice versa, at a wavelength of 1552.75 nm, the right sideband is suppressed by 17.5 dB compared to the left. These observations suggest that the WBG modulator acts as a single or vestigial sideband modulator [24], where the optical filter is directly integrated into the device and naturally matched in wavelength.

IV. Data Transmission Results

Fig. 3(a) shows the experimental setup for the data modulation and transmission experiments. We demonstrate NRZ-OOK modulation up to 100 Gbit/s, 25 GBd and 50 GBd 4PAM, as well as 25 GBd 8PAM, corresponding to data rates of 50, 100, and 75 Gbit/s, respectively.

A random bit sequence of the length 2^{17} is generated offline and loaded onto the memory of a digital-to-analog converter (DAC) with a sampling rate of 100 GSa/s, an output voltage peak of 250 mV and a 3 dB bandwidth of 35 GHz. The DAC's electrical output signal is amplified to a voltage peak of 0.9 V before being fed to the on-chip WBG modulator via a GS RF probe. Light from a TLS in the C-band is optionally pre-amplified by an erbium doped fiber amplifier (EDFA) to 17.9 dBm before being coupled to the chip. The collected light at the output is optionally transmitted through up to 12 km of standard singlemode fiber (SMF) and amplified by a second EDFA. The signal is detected by a 70 GHz pin-photodiode, directly mounted to a real-time oscilloscope (RTO) with a sampling rate of 160 GSa/s and an analog bandwidth of 63 GHz. Offline DSP is performed on the recorded signal and includes timing recovery, equalization, a hard symbol decision and bit error counting. The equalizing stage consists of an LMS-equalizer with 201 filter taps and an optional maximum a posteriori probability (MAP) equalization.

For the 25 Gbit/s (at 1559.2 nm) and 50 Gbit/s (at 1559.1 nm) signals, the pre-amplifier is omitted and an optical power of 13 dBm is fed to the chip. Bit error ratios (BERs) of below 10^{-6} and 1.9×10^{-6}, respectively, are measured. For the 100 Gbit/s NRZ-OOK measurements the laser power is amplified to 17.9 dBm before being coupled to the WBG modulator and a BER of 1.3×10^{-5} is obtained at an operational wavelength of 1559.05 nm. The corresponding eye diagrams after MAP equalization are displayed in Fig. 3(b).

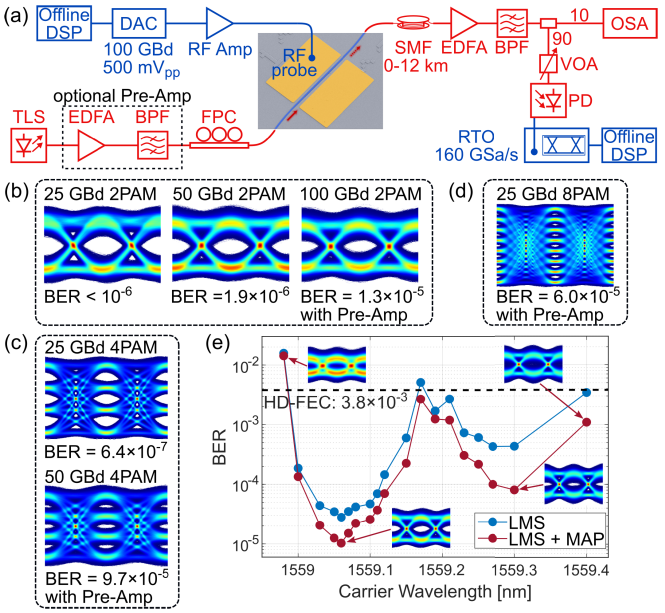

Fig. 3. (a) Experimental setup for high-speed data transmission measurements. (b) Eye diagrams for NRZ-OOK modulation at 25 Gbit/s, 50 Gbit/s and 100 Gbit/s. The measured BERs are displayed. (c), (d) Eye diagrams and BERs for 4-level and 8-level PAM signals at symbol rates of 25 GBd and 50 GBd. (e) BERs at different optical carrier wavelengths for a 100 Gbit/s NRZ-OOK signal with different digital signal processing (DSP) schemes at the receiver. Eye diagrams at highlighted carrier wavelengths are displayed as insets.

Additionally, higher-order modulation formats are tested. Fig. 3(c) shows the eye diagrams for a 25 GBd and a 50 GBd 4PAM signal, corresponding to data rates of 50 Gbit/s and 100 Gbit/s, and in Fig. 3(d) a 25 GBd 8PAM data modulation measurement is shown (data rate of 75 Gbit/s). The respective BERs are 6.4×10^{-7} and 9.7×10^{-5} for the 4PAM signals and 6.0×10^{-5} for the 8PAM signal. The laser wavelengths are set to 1559.15 nm (25 GBd 4PAM), 1559.19 nm (50 GBd 4PAM) and 1559.23 nm (25 GBd 8PAM).

Next, the operational wavelength range of an integrated WBG modulator is tested. In contrast to a balanced MZ-EOM, the WBG modulator relies on the electro-optic shift of a resonant wavelength. Hence, the modulator performance is strongly dependent on the carrier wavelength, making it susceptible to laser and thermal instabilities. 100 Gbit/s NRZ-OOK experiments are performed at varied laser carrier wavelength and the incident laser power is kept fixed at 17.9 dBm. In Fig. 3(d), the measured BERs for different offline DSP schemes at various carrier wavelengths are shown together with some exemplary eye diagrams as insets. For the blue data points, only a LMS equalization is performed, while for the red data points an additional MAP step improved the BERs at the cost of higher receiver complexity. These results

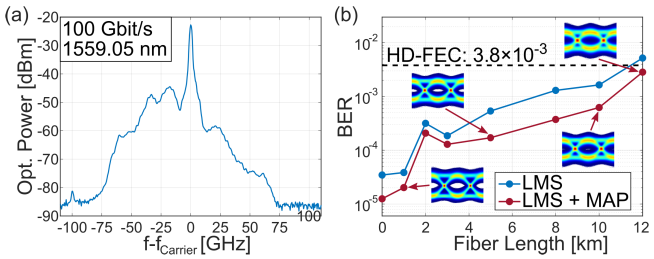

Fig. 4. (a) Optical spectrum of a 100 Gbit/s NRZ-OOK signal at a carrier wavelength of 1595.05 nm. (b) BERs at different transmission distances through a single mode fiber (SMF) after the WBG modulator. BERs lower than the HD-FEC threshold are measured up to 12 km of SMF. Eye diagrams at transmission distances of 1 km, 5 km, 10 km, and 12 km are shown as insets.

demonstrate that the integrated WBG modulator allows for data transmission rates of 100 Gbit/s with a BER below the hard-decision forward error correction (HD-FEC) threshold of 3.8×10^{-3} for wavelengths between 1559.0 nm and 1559.4 nm, hence over a wavelength range of 400 pm. The degradation of the modulation quality at the shorter wavelength side is caused by the strong filter response of the Bragg grating, which reduces the optical signal-to-noise-ratio at the receiver. At the longer wavelength side, the resulting phase modulation is not detected in an IM/DD setup. The best BER of 1.3×10^{-5} was found at a carrier wavelength of 1559.05 nm, where the modulator shows an excess insertion loss of 10 dB in the on-state. An alternative operating point at 1559.3 nm (BER of 8.1×10^{-5}) shows excess loss of only 1 dB. Alternatively, a DC bias can be introduced to optimize the modulator performance.

Lastly, data transmission experiments are performed to demonstrate the advantage of the WBG's inherent SSB modulation. Standard SMFs with lengths between 1 km and 12 km are introduced on the receiver side of the setup directly after the WBG modulator device [see Fig. 3(a)]. The modulator features a sideband suppression ratio of more than 10 dB for a 100 GBit/s NRZ-OOK signal centered at 1559.05 nm, as shown in Fig. 4(a). The measured BERs at different transmission link distances are plotted in Fig. 4(b) for a LMS equalization as well as for a LMS followed by a MAP equalization. The WBG allows for 100 Gbit/s data transmission below the HD-FEC threshold of 3.8×10^{-3} over 10 km with LMS, or 12 km with LMS and MAP equalization.

V. Conclusion

We demonstrated an integrated WBG modulator in LNOI with an optical extinction ratio of 53.8 dB at a Bragg wavelength of 1555.87 nm in the C-band, capable of modulating 100 Gbit/s NRZ-OOK signals with a BER of 1.3×10^{-5}. Additionally, multi-level modulation formats such as 4PAM and 8PAM at a symbol rate of 25 GBd and 4PAM at a symbol rate of 50 Gbd were transmitted. The optical carrier wavelength range allowing for operation below the HD-FEC limit was determined to be 400 pm. Transmission of a 100 Gbit/s NRZ-OOK signal over 12 km SMF in an IM/DD scheme without dispersion compensation is enabled by the WBG's SSB modulation, owed to its inherent optical filter characteristics.

Acknowledgment

The authors acknowledge the support for nanofabrication from the ScopeM and the cleanroom facilities BRNC and FIRST of ETH Zürich.

References

[1] D. A. B. Miller, "Attojoule optoelectronics for low-energy information processing and communications," *J. Lightw. Technol.*, vol. 35, no. 3, pp. 346–396, Feb. 1, 2017.
[2] D. Marpaung, J. Yao, and J. Capmany, "Integrated microwave photonics," *Nature Photon.*, vol. 13, no. 2, pp. 80–90, Feb. 2019.
[3] J. Yao, "Microwave photonics," *J. Lightw. Technol.*, vol. 27, no. 3, pp. 314–335, Feb. 1, 2009.
[4] P. J. Winzer and D. T. Neilson, "From scaling disparities to integrated parallelism: A decathlon for a decade," *J. Lightw. Technol.*, vol. 35, no. 5, pp. 1099–1115, Mar. 1, 2017.
[5] G. T. Reed, G. Mashanovich, F. Y. Gardes, and D. J. Thomson, "Silicon optical modulators," *Nature Photon.*, vol. 4, pp. 518–526, Jul. 2010.
[6] J. Liu *et al.*, "Waveguide-integrated, ultralow-energy GeSi electro-absorption modulators," *Nature Photon.*, vol. 2, no. 7, pp. 433–437, Jul. 2008.
[7] J. Leuthold *et al.*, "Silicon-organic hybrid electro-optical devices," *IEEE J. Sel. Topics Quantum Electron.*, vol. 19, no. 6, pp. 114–126, Dec. 2013.
[8] A. Messner *et al.*, "Plasmonic ferroelectric modulators," *J. Lightw. Technol.*, vol. 37, no. 2, pp. 281–290, Jan. 15, 2019.
[9] E. L. Wooten *et al.*, "A review of lithium niobate modulators for fiber-optic communications systems," *IEEE J. Sel. Topics Quantum Electron.*, vol. 6, no. 1, pp. 69–82, Jan. 2000.
[10] C. Wang *et al.*, "Integrated lithium niobate electro-optic modulators operating at CMOS-compatible voltages," *Nature*, vol. 562, no. 7725, pp. 101–104, Oct. 2018.
[11] M. He *et al.*, "High-performance hybrid silicon and lithium niobate Mach–Zehnder modulators for 100 Gbit s^{-1} and beyond," *Nature Photon.*, vol. 13, pp. 359–364, May 2019.
[12] C. Wang, M. Zhang, B. Stern, M. Lipson, and M. Lončar, "Nanophotonic lithium niobate electro-optic modulators," *Opt. Exp.*, vol. 26, no. 2, pp. 1547–1555, Jan. 2018.
[13] M. Li, J. Ling, Y. He, U. A. Javid, S. Xue, and Q. Lin, "Lithium niobate photonic-crystal electro-optic modulator," *Nature Commun.*, vol. 11, no. 1, Aug. 2020, Art. no. 4123.
[14] M. Xu, M. He, S. Yu, and X. Cai, "Thin-film lithium niobate modulator based on distributed Bragg grating resonators," in *Proc. Asia Commun. Photon. Conf.*, 2019, Paper S4D.5.
[15] S. Kaushal *et al.*, "Optical signal processing based on silicon photonics waveguide Bragg gratings: Review," *Frontiers Optoelectron.*, vol. 11, no. 2, pp. 163–188, Jun. 2018.
[16] S. Xie *et al.*, "Add–drop filter with complex waveguide Bragg grating and multimode interferometer operating on arbitrarily spaced channels," *Opt. Lett.*, vol. 43, no. 24, pp. 6045–6048, Dec. 2018.
[17] M. A. Baghban *et al.*, "Bragg gratings in thin-film $LiNbO_3$ waveguides," *Opt. Exp.*, vol. 25, no. 26, pp. 32323–32332, Dec. 2017.
[18] M. R. Escalé, D. Pohl, A. Sergeyev, and R. Grange, "Extreme electro-optic tuning of Bragg mirrors integrated in lithium niobate nanowaveguides," *Opt. Lett.*, vol. 43, no. 7, pp. 1515–1518, Apr. 2018.
[19] G. H. Smith, D. Novak, and Z. Ahmed, "Overcoming chromatic-dispersion effects in fiber-wireless systems incorporating external modulators," *IEEE Trans. Microw. Theory Techn.*, vol. 45, no. 8, pp. 1410–1415, Aug. 1997.
[20] B. Baeuerle *et al.*, "100 GBd IM/DD transmission over 14 km SMF in the C-band enabled by a plasmonic SSB MZM," *Opt. Exp.*, vol. 28, no. 6, pp. 8601–8608, Mar. 2020.
[21] J. T. Hastings, M. H. Lim, J. G. Goodberlet, and H. I. Smith, "Optical waveguides with apodized sidewall gratings via spatial-phase-locked electron-beam lithography," *J. Vac. Sci. Technol. B*, vol. 20, no. 6, pp. 2753–2757, 2002.
[22] D. Pohl *et al.*, "Tunable Bragg grating filters and resonators in lithium niobate-on-insulator waveguides," in *Proc. Conf. Lasers Electro-Opt.*, 2020, Paper STu4J.5.
[23] Y. Shi, L. Yan, and A. E. Willner, "High-speed electrooptic modulator characterization using optical spectrum analysis," *J. Lightw. Technol.*, vol. 21, no. 10, pp. 2358–2367, Oct. 2003.
[24] X. Wei and J. Leuthold, "Relation between vestigial-sideband filtering and $\pi/2$ progressive phase shift," *Opt. Lett.*, vol. 29, no. 14, pp. 1599–1601, Jul. 2004.